ACS NANO
Cite This: ACS Nano XXXX, XXX, XXX–XXX
www.acsnano.org

ARTICLE

Sensor-Instrumented Scaffold Integrated with Microporous Spongelike Ultrabuoy for Long-Term 3D Mapping of Cellular Behaviors and Functions

Hyungjun Kim,[†,∥] Min Ku Kim,[†,∥] Hanmin Jang,[‡,∥] Bongjoong Kim,[§] Dong Rip Kim,*[,‡] and Chi Hwan Lee*[,†,§,¥]

[†]Weldon School of Biomedical Engineering, Purdue University, 206 South Martin Jischke Drive, West Lafayette, Indiana 47907, United States

[‡]School of Mechanical Engineering, Hanyang University, 222 Wangsimni-ro, Seongdong-gu, Seoul 04763, Republic of Korea

[§]School of Mechanical Engineering, Purdue University, 610 Purdue Mall, West Lafayette, Indiana 47907, United States

[¥]Department of Speech, Language, and Hearing Sciences, Purdue University, West Lafayette, Indiana 47907, United States

Supporting Information

ABSTRACT: **Real-time monitoring of cellular behaviors and functions with sensor-instrumented scaffolds can provide a profound impact on fundamental studies of the underlying biophysics and disease modeling. Although quantitative measurement of predictive data for *in vivo* tests and physiologically relevant information in these contexts is important, the long-term reliable monitoring of cellular functions in three-dimensional (3D) environments is limited by the required set under wet cell culture conditions that are unfavorable to electronic instrument settings. Here, we introduce an ultrabuoyant 3D instrumented scaffold that can remain afloat on the surface of culture medium and thereby provides favorable environments for the entire electronic components in the air while the cells reside and grow underneath. This setting enables high-fidelity recording of electrical cell−substrate impedance and electrophysiological signals for a long period of time (weeks). Comprehensive *in vitro* studies reveal the utility of this platform as an effective tool for drug screening and tissue development.**

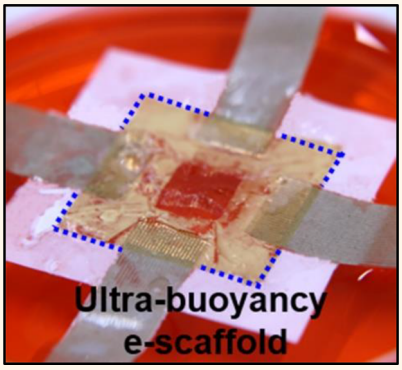

KEYWORDS: *instrumented scaffold, ultrabuoyancy, real-time 3D monitoring, cellular and tissue electrophysiology, tissue engineering*

The ability to record cellular behaviors and functions with high spatial and temporal resolutions enables fundamental understanding of the underlying biophysics and cellular electrophysiology.[1−5] Conventionally, the real-time monitoring of electrical activities of living cells occurs by using various sensing platforms such as optical imagers with voltage-sensitive dyes,[5] graphene-based sensors,[6] multiplexed electrode arrays,[7,8] and planar field-effect transistors (FETs),[9−11] but their spatial resolution remains limited because these methods are tailored for 2D cultured cells. The recent advent of injectable or rollable scaffold systems enables the spatially resolved 3D mapping of the cellular behaviors and functions in human tissue-mimicking environments.[12−14] Nonetheless, challenges remain for their long-term, high-fidelity recording due to the lack of effective means to electrically decouple all of the necessary electronic instrument settings from submerged conditions in a cell culture medium including oxygen, pH, conductivity, and/or agitation, which often requires additional packaging to prevent wetting and damaging.[15]

Here, we report a 3D-stackable electronic scaffold (e-scaffold) integrated with an engineered ultrabuoy that allows the entire structure to remain afloat on the surface of medium and therefore offers favorable environments for both biological cells and electronics. The e-scaffold system contains multimodal arrays of sensing elements in vertically stackable configurations, providing the capability for spatially resolved 3D mapping of cellular behaviors and functions. Demonstrations of the e-scaffold system in 3D mapping of cellular impedances and cardiac action potentials from cancer and cardiomyocyte cells with high fidelity over weeks illustrate the utility of this concept. Comprehensive *in vitro* studies reveal

Received: March 24, 2019
Accepted: June 19, 2019
Published: June 19, 2019

DOI: 10.1021/acsnano.9b02291
ACS Nano XXXX, XXX, XXX–XXX

the important features of the underlying materials, design rules, operational arrangements, and all of the relevant aspects of operations.

RESULTS AND DISCUSSION

Basic Configuration of the e-Scaffold System. Figure 1a shows an exploded schematic view (left) and an optical image (right) of the e-scaffold system afloat on a cell culture medium (Eagle Medium, Gibco). The basic components of the e-scaffold system include (1) multimodal arrays of sensing elements to detect electrical cell−substrate impedance and/or electrophysiological signals, (2) thin films (<1 μm thick) of waterproof polyimide (PI) elastomer to serve as the substrate and encapsulation, (3) high concentration of cold matrigel (20 mg/mL, Corning) surrounding the entire e-scaffold to serve as the matrix that contains biological cells, (4) flexible anisotropic conductive film (ACF) cables (HST-9805-210, Elform, Inc., USA) to connect the e-scaffold with an external data acquisition unit, and (5) a sheet of highly water-repellent ultrabuoy that consists of microporous spongelike polydimethylsiloxane (PDMS) with an effective specific weight of ~456 kg/m^3 that is >4 times lower than the cell culture medium (~1926 kg/m^3), all anchored to the peripheral area of the e-scaffold. In this configuration, all of the electronic components including the ACF cables remain on the top of the spongelike PDMS to avoid wetting, while cells can reside and grow underneath the e-scaffold in the submerged culture conditions. To further promote the ultrafloatation capability, the spongelike PDMS is additionally incorporated with polytetrafluoroethylene (PTFE) nanoparticles (NPs, 0.2−5 μm diameter) covered by a thin layer of medical-grade Teflon (AF2400, DuPont, USA), leading to a substantial increase of the buoyancy force and the surface tension by >20% and >35%, respectively (Figure 1b). This ultrafloatation capability allows the e-scaffold to keep out of the medium even against intentional pressing up to ~51 N/m^2 (Figure 1c and movie S1) while continuously offering favorable environments for both electronics and cells. A series of scanning electron microscope (SEM) images of the spongelike PDMS appear in Figure 1d, highlighting the internal features. Further characterizations of the spongelike PDMS in terms of the effective specific weight, contact angle, dynamic droplet behavior, and critical immersion weight and depth appear in Figure S1, with the summarized results in Table S1. Figure S2 presents experimental results showing that the electrical impedance of the e-scaffold system remains nearly unaffected when deployed on the surface of the cell medium in an incubator (Midi CO_2 Incubators, Thermo Scientific, USA) at 37 °C under an atmosphere with 5% of CO_2 over 2 weeks, whereas abrupt reduction of the impedance occurs within a short period of time in the control groups without the microporous spongelike ultrabuoy and with a conventional encapsulation using untreated (nonporous) PDMS due to short-circuit paths by wetting and penetration of the cell media.

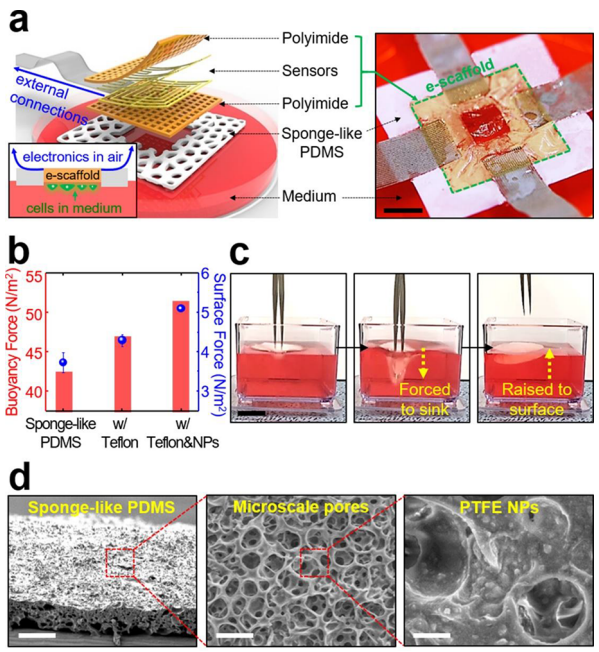

Figure 1. Basic configuration of the e-scaffold system: (a) exploded schematic view (left) and optical image (right) of the e-scaffold system afloat on a cell culture medium. Scale bar is 1 cm. (b) Results of the buoyancy and surface tension forces of the e-scaffold system. (c) Sequential optical images of microporous spongelike PDMS coated with Teflon and PTFE NPs floating on a cell culture medium against intentional force. Scale bar is 3 cm. (d) SEM images of the microporous spongelike PDMS. Scale bars are 90, 60, and 10 μm from the left.

Cell Compatibility and 3D Construction. Cell compatibility of the e-scaffold system is a key consideration for its implementation in 3D cell culture and tissue engineering applications.[16−19] Figure 2a (red bars) presents representative results of a cell compatibility assay (MTT, Sigma-Aldrich, USA) for the e-scaffold system seeded with green fluorescent protein (GFP)-expressed MCF7 cells and floated upside down on the medium. Prior to the cell seeding, the e-scaffold system along with the spongelike PDMS was sterilized with 70% (v/v) ethanol for 30 min and dried under ultraviolet (UV) irradiation for 1 h and then stored in an incubator (Midi CO_2 Incubators, Thermo Scientific, USA) at 37 °C under an atmosphere with 5% of CO_2. The results show that the proliferation rate of the cells increases consistently throughout the assay period (2 days) while displaying no substantial difference compared to those obtained from a control group without any electronics embedded inside (black bars). Figure 2b shows the corresponding confocal fluorescence microscope images (A1Rsi confocal microscope, Nikon) of a monolayer of the cells at day 2, wherein the yellow dashed lines indicate the embedded recording electrodes (Au, 150 nm). The cells become confluent and start to cover the e-scaffold system when the size of the mesh holes is smaller than 200 μm. Nonuniform distribution of the cells appears in the specimens that exhibit the mesh hole size of >300 μm (Figure S3). A control experiment on green immunofluorescence stained cardiomyocyte cells at the 8-day incubation produces consistent results (Figure 2c), confirming that the e-scaffold system is conducive to cell growth, proliferation, and extracellular matrix formation. Details about the cell culture and associated experimental procedures appear in the Methods.

Another interesting aspect is that the e-scaffold system can be stacked multiple layers within a single matrigel, providing the desired 3D cell culture environments where cells can grow and interact with the surrounding environment in all dimensions to form tissues for a variety of tissue-engineering applications.[16−19] Figure 2d presents pilot data obtained from the four-layer-stacked e-scaffold system surrounded with dense

DOI: 10.1021/acsnano.9b02291
ACS Nano XXXX, XXX, XXX−XXX

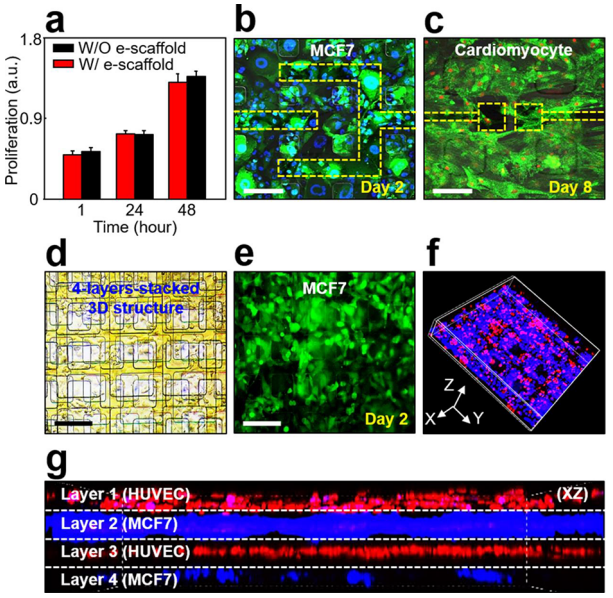

Figure 2. Cell compatibility and 3D construction. (a) Results of MTT assays for GFP-MCF7 cells seeded on the e-scaffold system. (b) Conformal fluorescence microscope image of the monolayer of the GFP-MCF7 cells at 2-day incubation (green = GFP, blue = DAPI). Scale bar is 100 μm. (c) Results of control experiments with green immunofluorescence stained cardiomyocyte cells at 8-day incubation (green = FITC, red = Draq5). Scale bar is 60 μm. (d) Optical image of the four-layers-stacked e-scaffold system surrounding with dense cell (MCF7) layers after 3-day incubation. Scale bar is 200 μm. (e) Confocal fluorescence microscope image of the stacked e-scaffold system (green = GFP). Scale bar is 200 μm. (f, g) Tilted and side view of the stacked e-scaffold system with alternatively stacked GFP-MCF7 cells and GFP-HUVEC cells (blue = DAPI, red = Draq5).

cell (MCF7) layers after the 3-day incubation with the corresponding confocal fluorescence microscope image in Figure 2e. The results consistently indicate that the e-scaffold system supports cell growth and tissue formation. Furthermore, alternative stacking of the e-scaffold system seeded with a specific sequence of different cells is possible, thereby yielding a 3D heterocellular structure.[20−22] Parts f and g of Figure 2 show representative confocal fluorescence microscopy images for the e-scaffold system with alternately stacked cancer cells (*e.g.*, GFP-MCF7) and endothelial cells (*e.g.*, GFP-HUVEC cells). Each cell layer is separately incubated for 2 days under different culture conditions and then stained with DAPI and Draq5 for the MCF7 and HUVEC cells, respectively. The corresponding top view images in Figure S4 highlight the confluent layers of the well-attached cells with normal morphologies. The formation of vascular tubes in the HUVEC cells occurs, exhibiting extensive branches with a typical length of 80 μm at day 3 (Figure S5). The subsequent treatment of both vascular endothelial growth factor (VEGF) and fibroblast growth factor (β-FGF) remains required to form the tumor vasculature, thereby allowing for more systematic investigations.[23,24]

Real-Time Monitoring of Electrical Cell−Substrate Impedance. Real-time monitoring of electrical cell−substrate impedance presents a nonlabeling technique to understand cellular functions such as adhesion, growth, differentiation, mitigation, and drug effect on cell behaviors.[25] Biological cells serve as dielectric particles due to the insulating properties of their membranes, and therefore, their attachment and detachment affect the current flow between the recording electrodes, leading to distinguishable changes in the impedance values.[26] To illuminate this capability, a model e-scaffold system is constructed into a configuration of interdigitated arrays (width 80 μm, gap 100 μm) of the embedded recording electrodes (Au, 150 nm) for the measurement of electrical impedance (Figure S6). The equivalent circuit model appears in Figure S7a, showing the recording electrode resistance (R_E), cell culture medium (R_{medium}), Helmholtz double-layer interfacial capacitance (C_I), and additional resistance (R_{cells}) and capacitance (C_{cells}) by the introduction of cells. The recording electrodes act as a normal capacitor wherein the resulting impedance ($X_c = 1/(j\omega C)$, $C = (\varepsilon_r\varepsilon_0 A)/d$) is subject to frequency (ω), dielectric constant (ε_r) of the surrounding materials (air = 1.00059, water = 80.4, medium = 80), cross-sectional area of the recording electrode (A = ∼3900 μm^2), and gap between the interdigitated arrays (d = 100 μm). A representative frequency−impedance curve of the e-scaffold system at a frequency range of 1−250 kHz appears in Figure S7b. Details about the measurement of cellular impedance appear in the Methods.

Figure 3a shows representative SEM (left), microscopy (middle), and conformal microcopy (right) images of the model e-scaffold system within a matrigel seeded with MCF7 cells after 1 h of incubation. The e-scaffold system remains afloat on the medium, wherein the recording electrodes are entirely surrounded by the PI elastomers. The ACF cables placed on the spongelike PDMS are wired to an external data acquisition system (E4980AL Precision LCR meter, Keysight Technologies, USA) through the air. Figure 3b shows the results of time-dependent impedance obtained separately from MCF7 cells (black line), SKOV3 cells (red line), and HUVEC cells (green line) for 50 h during the period of growth and proliferation. The results show that the impedance increases linearly for the first ∼4 h when the cells start to settle down and become adherent to the recording electrodes, implying that the cells act as an electrical insulating medium.[27] From ∼16 h later, a drastic increase of the impedance occurs due to the cell aggregation and continuous proliferation. This tendency is more obvious in the MCF7 cells because the population doubling time of MCF7 cells (∼29 h) is shorter than that of SKOV3 cells (∼48 h) and HUVEC cells (∼60 h). Consistently, the impedance of the MCF7 cells increases proportionally to the cellular density (Figure 3c). An impedimetric cytotoxicity plot for the MCF7 cells appears in Figure 3d, while a model drug such as a hydrophilic and water-soluble doxorubicin (Dox, doxorubicin hydrochloride, Fisher, USA, solubility ∼50 mg/mL) is introduced in the medium with different dosages at 1-day incubation. The results reveal that the impedance starts to decrease within ∼4 h after the drug administration (100 μM) when the effect of the Dox becomes apparent and eventually leads to cell death and detachment (Figure S8). It is observed that no substantial decrease of the impedance appears in the control groups with the low drug administration (10 μM).

Stacking the e-scaffold systems multiple times provides the capability of monitoring spatially resolved impedance from cultured cells in 3D-structured environments.[28] Figure 3e shows a schematic illustration for the three-layer-stacked e-scaffold system within a single matrigel seeded with MCF7 cells, which is floated upside down on the medium by using the spongelike PDMS. In this configuration, each layer of the e-

DOI: 10.1021/acsnano.9b02291
ACS Nano XXXX, XXX, XXX−XXX

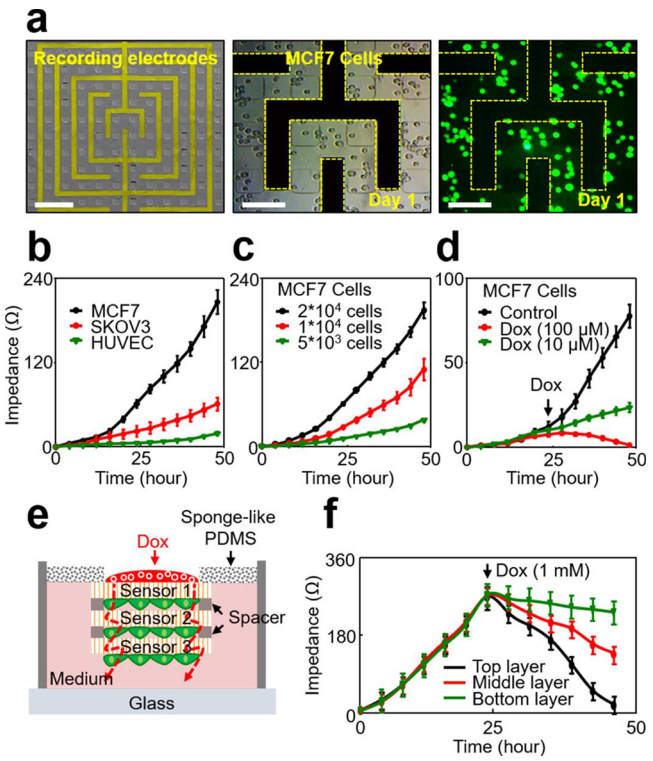

Figure 3. Real-time monitoring of electrical cell−substrate impedance. (a) Representative SEM (left), microscopy (middle), and conformal microcopy (right) images of the e-scaffold system embedded with impedance sensors (green = GFP). Scale bars are 300, 100, and 100 μm from the left. (b) Results of the time-dependent impedance for the MCF7 cells (black line), SKOV3 cells (red line), and HUVEC cells (green line) for 50 h. (c) Corresponding results of the different density of the MCF7 cells. (d) Impedimetric cytotoxicity plot for the MCF7 cells with the administration of Dox. (e) Schematic illustration for the three-layer-stacked e-scaffold system within a single matrigel seeded with MCF7 cells. (f) Results of the real-time monitoring of the impedances. Data are presented as means ± SE (n = 3).

scaffold system remains spaced apart a fixed distance of ∼5 mm along the perimeter by using spacers made of PDMS. Figure 3f shows the time-dependent impedance obtained from each layer of the e-scaffold system on the top (black line), middle (red line), and bottom (green line), while 1 mM of Dox is introduced on the uppermost top at the 1-day incubation. The impedance increases at nearly the same rate during the cell growth and proliferation and then abruptly decreases following the drug administration with different rates (top: ∼10.1 Ω/h, middle: ∼5.4 Ω/h, bottom: ∼1.6 Ω/h), as the Dox molecules diffuse downward from the top within the matrigel. These results are consistent with the confocal fluorescence microscopy images (Figure S9) obtained from the top (left image), middle (middle image), and bottom (right image) layer of the e-scaffold system at 12 h after the treatment of Dox (1 mM), indicating that the top layer contains the most Dox, followed by the middle and bottom layers. This platform for the real-time impedimetric analysis of drug-induced cellular events in 3D environments can provide important insights into the mechanism of complex cellular phenomena for the identification of diseased cells at different stages and their interactions with therapeutic agents.[29]

Real-Time 3D Monitoring of Cardiac Action Potential. Real-time 3D monitoring of electrophysiological signals in electrically active cells such as the heart, brain, and muscle cells enables spatially resolved quantitative analysis of action potential propagations to understand tissue development, drug modulation, and functions of diseased or damaged tissues.[13,30] To demonstrate the potential use of the e-scaffold system in this context, a model three-layer-stacked e-scaffold system is constructed within a single matrigel containing cardiomyocytes and tailored for the detection of electrocardiography (ECG) signals. Each layer of the e-scaffold system consists of 36 recording electrodes (Au, 150 nm, width = 60 × 60 μm^2, electrode gap = 10 μm, distance between the recording electrodes = 1150 μm) (Figure S10a). In this configuration, the monitoring of the cellular contractions occurs on each recording electrode, while the array-type mapping reveals the spatial distributions and variations of the cardiomyocyte throughout the 3D environment. The cardiomyocytes undergo maturation in culture, leading to formation of a tissue layer aligned to the e-scaffold system at day 8 in vitro (Figure S10b). The representative immunostained confocal images of cardiomyocytes stained with sarcomeric α-actinin taken from several different areas after 8 days of incubation (Figure S10c) reveal that cardiomyocytes are homogeneously distributed along the surface and elongated with high aspect ratios, providing information on the maturation of cells and formation of tissues with hallmarks of the native myocardium. As the cardiomyocytes mature, the sarcomeres assemble in series to form myofibrils that extend across the cells wherein the myofibrils are anchored to the ends of the cardiomyocytes by the cell−cell junctional structure.

Figure 4a shows the recorded ECG signals in real time from the cardiomyocytes at the day 2, 6, and 8, exhibiting the typical shape of cardiac action potential signals at frequencies of 4.8, 1, and 0.6 Hz, respectively. The beating rate decreases from 288 to 60 bpm and to 36 bpm, whereas the amplitude increases from 66 to 83 μV and to 511 μV at day 2, 6, and 8, respectively (movies S2, S3, and S4). The results imply that spontaneous contractions of the individual cells initially occur, followed by stronger and more synchronized contractions as the cells become more in contact with each other. Figure 4b shows the continuously recorded ECG signals from the cardiomyocytes at day 8 in response to the addition of 100 μL of norepinephrine (NE) into the medium, displaying that the beating rate increases nearly 2-fold within ∼3 min after the NE administration. A representative microscopy image in Figure 4c highlights the embedded four-channel-multiplexed sensing electrodes with the cardiomyocytes at day 8 within the domain of 1.4 × 1.4 mm^2 (movie S5). The results in Figure 4d show the synchronized beating rate (∼0.63 Hz), amplitude (638−763 μV), and peak width (∼1.6 s), which are within the range of those reported in previous studies.[9,13] The 3D mapping results of the action potentials (Figure 4e) obtained from the total 48 ECG sensors (4 × 4 array in each layer) reveal the spontaneous beating activities of the cardiomyocytes at day 2, 6, and 8, without showing any toxic effect.

CONCLUSION

The results presented here demonstrate that the e-scaffold integrated with the microporous spongelike ultrabuoy on medium allows long-term, high-fidelity monitoring of cellular behaviors and functions in favorable environments for both biological cells and electronics. The physical stacking of the e-scaffold system enables the incorporation of large numbers of addressable sensors in a multidirectional arrangement, offering

DOI: 10.1021/acsnano.9b02291
ACS Nano XXXX, XXX, XXX−XXX

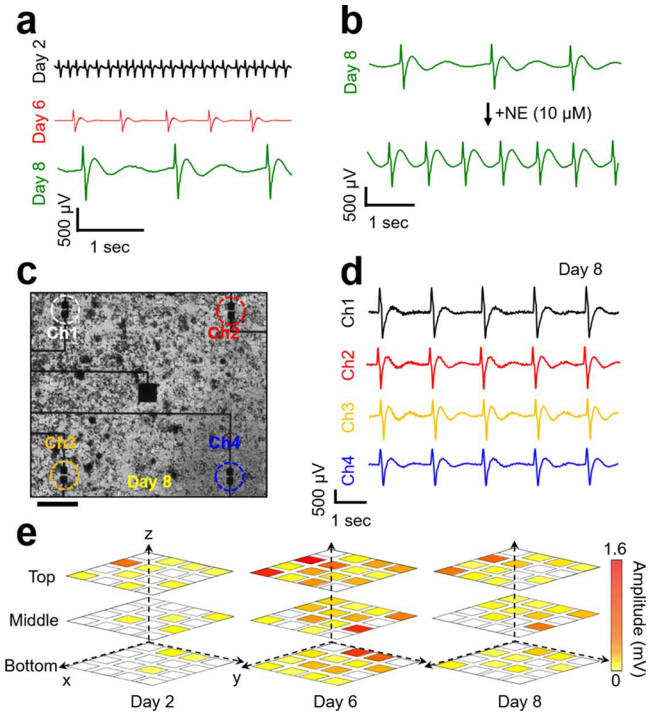

Figure 4. 3D mapping of cardiac action potential. (a) Results of the ECG signals recorded from the cardiomyocytes at days 2, 6, and 8. (b) Continuously recorded ECG signals recorded from the cardiomyocytes at day 8 in response to the addition of 100 μL of norepinephrine (NE) into the medium. (c) Representative microscopy image of the embedded four-channel-multiplexed ECG sensors with cardiomyocytes at day 8. Scale bar is 200 μm. (d) Results for the synchronized beating of the cardiomyocytes at day 8. (e) Results of the 3D mapping of the action potentials of cardiomyocytes at days 2, 6, and 8 from the left.

the 3D mapping capability. These findings suggest an expanded set of potential options such as long-term stable monitoring of tissue functions during/after *in vivo* transplant to replace diseased or damaged tissues.[31] The real-time monitoring of the cellular behaviors and functions with temporal resolutions during endothelial lumen formation in tumor tissue or during the invasion of SKOV3 cells into HUVEC cells to obtain information on their interactions between invading cancer cells and the adherent cells would be highly desired, suggesting directions for future research.[32−34] It might be also interesting to consider constructing a bioresorbable form of the e-scaffold system such that the constituent materials degrade harmlessly in the body following implantation and after a clinically useful period, thereby eliminating the need for postsurgical extraction.[35−38] Although this study focuses on the advantages provided by impedance and electrophysiological sensor, similar systems instrumented with more diverse sensing modalities, such as detection of pH, pressure, temperature, and/or mechanical strains, can be considered.[39−41]

MATERIALS AND METHODS

Fabrication of the e-Scaffold System. The fabrication began by spin-casting the layers of PMMA (1 μm thick) and PI (1 μm thick) on a Si substrate. Thin films of Cr/Au film (5 nm/150 nm) were deposited by using an electron-beam (e-beam) evaporator. A photolithographic patterning with a photoresist (AZ 1518, 3000 rpm, 30 s) and subsequent wet etching steps in solutions of Cr and Au etchants (Transene, Inc.) followed to define the metallic thin film electrodes and the interconnecting traces. The encapsulation layer of PI (1 μm thick) was spin-casted on top and patterned by photolithography with a photoresist (AZ 9260, 3000 rpm, 1 min) and oxygen (O_2) plasma reactive ion etching (RIE) to define the basic structure of the e-scaffold system.

Fabrication of the Microporous Spongelike Ultrabuoy. The fabrication began by spin-casting a mixture of PDMS base material and curing agent (10:1 weight ratio) on a glass substrate at 100 rpm for 10 min. The as-prepared PDMS was then placed into a pressure cooker maintained at the preset pressure (90 kPa) and temperature (100 °C) for 20 min. The microscale pores were formed during the high-pressure steaming step while the PDMS was completely polymerized, providing the superhydrophobicity and antiwetting performance. The resulting microporous spongelike PDMS was dried in a convection oven at 70 °C for 1 h to remove the residual water molecules. A solution of Teflon (1 wt % AF2400, Dupont, USA) mixed with PTFE nanoparticles (0.2−5 μm, Polysciences, Inc. and Sigma-Aldrich, USA) was spin-casted at 1000 rpm for 5 min and then cured at 150 °C on a hot plate to increase the surface tension force, leading to increased static water contact angle and decreased effective surface adhesion against cell medium.

Measurement of Static Contact Angle and Dynamic Droplet. The static contact angle was measured by placing a droplet (∼10 μL) of distilled (DI) water and oil on a specimen by using a computer-controlled contact angle analyzer (Surface Electro Optics, Phoenix-10). The dynamic droplet behaviors of DI water and oil when dropped (∼15 μL) from a height of ∼4 cm were monitored by using a high speed camera at 50 frames per second.

Measurement of Buoyancy Force. The buoyancy force was measured by adding equally balanced weights (∼0.25 g) one after another on the top surface of a specimen afloat on the culture medium (RPMI1640, Sigma-Aldrich, USA). The total supporting buoyancy force was estimated according to the critical weight by which the specimen was immersed.

Cell Compatibility Assay. The specimens were sterilized by soaking in 70% (v/v) ethanol for 30 min and rinsing twice with phosphate buffer saline (PBS) followed by dehydration under UV irradiation for 1 h. The specimens were treated with O_2 plasma (35 W, 3 min) and immersed in fibronectin/gelatin solution (0.5% fibronectin, F1141, Sigma-Aldrich, USA, and 0.02% gelatin, Fisher Scientific, USA) for 1 day. The cells suspended in 50% medium and 50% Matrigel (Corning Life Sciences, USA) were then seeded on the specimens. In order to assess the cell proliferation, ∼5 × 10^3 cells were seeded and incubated. After the incubation, 3-(4,5-dimethylthiazol-2-yl)-2,5-diphenyltetrazolium bromide (MTT, Sigma-Aldrich, USA) was added to the cells, and the fluorescent intensity was measured at 580 nm by using a microplate reader (SpectraMax Plus 384 reader, Molecular Devices, USA). For the confocal microscopy analysis, the cells were fixed with 4% v/v paraformaldehyde in PBS for 15 min, stained with DAPI (500 nM, Invitrogen, USA) or Draq5 (1 μM, Invitrogen, USA) for 2 min, and mounted with an antifade reagent. The resulting cells were imaged by using the A1Rsi confocal microscope (Nikon, Japan).

Cardiomyocyte Isolation. Primary neonatal mice cardiomyocytes were prepared according to the Pierce Primary Cardiomyocyte Isolation Kit (Thermo Scientific, USA). Briefly, neonatal hearts were isolated from 1−3 day old neonatal mice and placed into separate sterile microcentrifuge tubes containing 500 μL of ice-cold Hank's Balanced Salt Solution (HBSS). Each isolated heart was then minced into 1−3 mm^3 pieces and washed twice with 500 μL of ice-cold HBSS to remove blood from the tissue. The minced tissues were incubated with 200 μL of reconstituted Cardiomyocyte Isolation Enzyme 1 (with papain) and 10 μL of Cardiomyocyte Isolation Enzyme 2 (with thermolysin) to each tube in an incubator at 37 °C for 30 min. After the incubation, the tissues were removed from the enzyme solution and washed twice with 500 μL of the ice-cold HBSS and 500 μL of complete Dulbecco's modified Eagle's medium (DMEM) was added for primary cell isolation to the tissues. The cardiomyocytes (6 × 10^6) were seeded onto a specimen with 50% medium and 50% matrigel

DOI: 10.1021/acsnano.9b02291
ACS Nano XXXX, XXX, XXX−XXX

(Corning Life Sciences, USA). The cell constructs were supplemented with complete DMEM for primary cell isolation and further incubated.

Immunostaining. For the cardiomyocyte immunostaining, the cardiomyocytes were fixed with 4% paraformaldehyde (Electron Microscope Sciences, USA) in PBS for 30 min and then washed three times with PBS. The cardiomyocytes were incubated with 0.25% Triton X-100 (Sigma-Aldrich, USA) in PBS for 1 h and washed three times with ice-cold PBS and preblocked for 1 h at room temperature in PBS containing 10% FBS, after which the specimens were washed three times with PBS. The specimens were incubated with primary antisarcomeric α-actinin mouse monoclonal antibodies (1:250; Sigma-Aldrich, USA) in SuperBlock (TBS) blocking buffer solution (Thermo Scientific, USA) for 1 h at room temperature, washed three times, and then incubated with AlexaFluor-488 goat antimouse secondary antibody (1:400; Invitrogen, USA) for 1 h, followed by rinsing with PBS. For the cell nuclei staining, the cardiomyocytes were stained with 1 μM of Draq5 for 2 min and then rinsed with PBS. The resulting specimens were imaged by using the A1Rsi confocal microscope (Nikon, Japan).

Measurement of Impedance. The impedance was measured by using an LCR meter (Agilent 4294A, USA) with a voltage (between two adjacent recording electrodes) of ~1 mV for 48 h at frequencies of 1, 5, 10, 20, 30, 50, 100, 150, 200, and 250 kHz, respectively. The e-scaffold system was placed in the incubator (5% CO_2, 37 °C; Thermo Scientific, USA) and wired to the LCR meter located outside of the incubator *via* flexible ACF cables. The data were collected every 2 h from the e-scaffold system. The frequency responses of the cytotoxic effects were obtained by measuring the impedance of the MCF7 cells treated with different doses of Dox at the frequency of 30 kHz.

Measurement of ECG Signals. The ECG signals of the cardiomyocytes were acquired by using the multichannel electrophysiological data acquisition unit (BioRadio, USA) with a notch filter (60 Hz) and a custom filter (Filter type: Bandpass, Filter design: Butterworth, order: 4, lower cutoff: 0.5, upper cutoff: 10). The e-scaffold system was placed in the incubator (5% CO_2, 37 °C; Thermo Scientific, USA) and wired to the data acquisition unit *via* flexible ACF cables. The data were collected at a sample rate of 2 kHz through differential programmable channels and then postprocessed using commercial software (BioCapture). The solution of norepinephrine bitartrate (10 μM; Sigma-Aldrich, USA) was used to increase the beating rate of the cardiomyocytes.

ASSOCIATED CONTENT

Supporting Information

The Supporting Information is available free of charge on the ACS Publications website at DOI: 10.1021/acsnano.9b02291.

Ultrafloatation capability of the e-scaffold (MP4)

Spontaneous beating of the cardiomyocyte monolayer at day 2 (MP4)

Spontaneous beating of the cardiomyocyte monolayer at day 6 (MP4)

Spontaneous beating of the cardiomyocyte monolayer at day 8 (MP4)

Synchronized beating of the cardiomyocyte monolayer on four-channel-multiplexed e-scaffold at day 8 (MP4)

Summary of characterization of microporous spongelike PDMS (Figure S1); impedance measurement of e-scaffold system with spongelike ultrabuoy, conventional encapsulation, and any buoy (Figure S2); confocal images of GFP-MCF7 cells on e-scaffold with different mesh pore size (Figure S3); confocal images of GFP-MCF7 and GFP-HUVEC cells on the four-layer-stacked e-scaffold (Figure S4); confocal image of tube formation of GFP-HUVEC cells on the e-scaffold (Figure S5); schematic and SEM image of impedance sensor and confocal image of GFP-MCF7 cells on e-scaffold (Figure S6); equivalent circuits and frequency measurement of impedance sensor (Figure S7); confocal images of GFP-MCF7 cells with and without Dox on impedance sensor (Figure S8); confocal images of three-layered stacked e-scaffold at 12 h after Dox treatment (Figure S9); schematic and SEM image of ECG sensor and confocal images of immunostained cardiomyocytes on e-scaffold (Figure S10); summary of the experimental results for spongelike PDMS (Table S1) (PDF)

AUTHOR INFORMATION

Corresponding Authors

*E-mail: lee2270@purdue.edu.

*E-mail: dongrip@hanyang.ac.kr.

ORCID

Hanmin Jang: 0000-0002-7724-4244

Dong Rip Kim: 0000-0001-6398-9483

Chi Hwan Lee: 0000-0002-4868-7054

Author Contributions

‖H.K., M.K.K., and H.J. contributed equally to this work.

Notes

The authors declare no competing financial interest.

ACKNOWLEDGMENTS

We thank S. Harbin and D. H. Kim for the inspiring discussion on tissue engineering. C.H.L. acknowledges funding support from the Asian Office of Aerospace Research & Development (AOARD: FA2386-16-1-4105) and the Air Force Office of Scientific Research (AFOSR: FA2386-18-1-40171) and support from the College of Engineering at Purdue University. D.R.K. acknowledges funding support from the International Research and Development Program (NRF-2018K1A3A1A32055469) through the National Research Foundation of Korea (NRF) funded by the Ministry of Science and ICT of Korea. D.R.K. also acknowledges financial support from the Intelligent Synthetic Biology Center of Global Frontier Project (NRF-2012M3A6A8054889) and the Basic Science Research Program (NRF-2015R1C1A1A02037752) funded by the Ministry of Science and ICT of Korea.

REFERENCES

(1) Rotenberg, M. Y.; Tian, B. Z. Talking to Cells: Semiconductor Nanomaterials at the Cellular Interface. *Adv. Biosyst.* **2018**, *2*, 1700242.

(2) Tian, B.; Cohen-Karni, T.; Qing, Q.; Duan, X.; Xie, P.; Lieber, C. Three-Dimensional, Flexible Nanoscale Field-Effect Transistors as Localized Bioprobes. *Science* **2010**, *329*, 830−834.

(3) Fu, T. M.; Hong, G. S.; Viveros, R. D.; Zhou, T.; Lieber, C. M. Highly Scalable Multichannel Mesh Electronics for Stable Chronic Brain Electrophysiology. *Proc. Natl. Acad. Sci. U. S. A.* **2017**, *114*, 10046−10055.

(4) Zhou, T.; Hong, G.; Fu, T. M.; Yang, X.; Schuhmann, T. G.; Viveros, R. D.; Lieber, C. M. Syringe-Injectable Mesh Electronics Integrate Seamlessly with Minimal Chronic Immune Response in the Brain. *Proc. Natl. Acad. Sci. U. S. A.* **2017**, *114*, 5894−5899.

(5) Cohen-Karni, T.; Timko, B. P.; Weiss, L. E.; Lieber, C. M. Flexible Electrical Recording from Cells using Nanowire Transistor Arrays. *Proc. Natl. Acad. Sci. U. S. A.* **2009**, *106*, 7309−7313.

(6) Kleber, A. G.; Rudy, Y. Basic Mechanisms of Cardiac Impulse Propagation and Associated Arrhythmias. *Physiol. Rev.* **2004**, *84*, 431−488.

(7) Kim, S. J.; Cho, H. R.; Cho, K. W.; Qiao, S. T.; Rhim, J. S.; Soh, M.; Kim, T.; Choi, M. K.; Choi, C.; Park, I.; Hwang, N. S.; Hyeon, T.; Choi, S. H.; Lu, N. S.; Kim, D. H. Multifunctional Cell-Culture Platform for Aligned Cell Sheet Monitoring, Transfer Printing, and Therapy. *ACS Nano* **2015**, *9*, 2677−2688.
(8) Feiner, R.; Fleischer, S.; Shapira, A.; Kalish, O.; Dvir, T. Multifunctional Degradable Electronic Scaffolds for Cardiac Tissue Engineering. *J. Controlled Release* **2018**, *281*, 189−195.
(9) Feiner, R.; Engel, L.; Fleischer, S.; Malki, M.; Gal, I.; Shapira, A.; Shacham-Diamand, Y.; Dvir, T. Engineered Hybrid Cardiac Patches with Multifunctional Electronics for Online Monitoring and Regulation of Tissue Function. *Nat. Mater.* **2016**, *15*, 679−685.
(10) Timko, B. P.; Cohen-Karni, T.; Yu, G. H.; Qing, Q.; Tian, B. Z.; Lieber, C. M. Electrical Recording from Hearts with Flexible Nanowire Device Arrays. *Nano Lett.* **2009**, *9*, 914−918.
(11) Duan, X.; Gao, R.; Xie, P.; Cohen-Karni, T.; Qing, Q.; Choe, H. S.; Tian, B.; Jiang, X.; Lieber, C. M. Intracellular Recordings of Action Potentials by an Extracellular Nanoscale Field-Effect Transistor. *Nat. Nanotechnol.* **2012**, *7*, 174−179.
(12) Ingebrandt, S.; Yeung, C. K.; Staab, W.; Zetterer, T.; Offenhausser, A. Backside Contacted Field Effect Transistor Array for Extracellular Signal Recording. *Biosens. Bioelectron.* **2003**, *18*, 429−435.
(13) Dai, X. C.; Zhou, W.; Gao, T.; Liu, J.; Lieber, C. M. Three-Dimensional Mapping and Regulation of Action Potential Propagation in Nanoelectronics-Innervated Tissues. *Nat. Nanotechnol.* **2016**, *11*, 776−782.
(14) Tian, B. Z.; Liu, J.; Dvir, T.; Jin, L. H.; Tsui, J. H.; Qing, Q.; Suo, Z. G.; Langer, R.; Kohane, D. S.; Lieber, C. M. Macroporous Nanowire Nanoelectronic Scaffolds for Synthetic Tissues. *Nat. Mater.* **2012**, *11*, 986−994.
(15) Bonk, S. M.; Stubbe, M.; Buehler, S. M.; Tautorat, C.; Baumann, W.; Klinkenberg, E. D.; Gimsa, J. Design and Characterization of a Sensorized Microfluidic Cell-Culture System with Electro-Thermal Micro-Pumps and Sensors for Cell Adhesion, Oxygen, and pH on a Glass Chip. *Biosensors* **2015**, *5*, 513−536.
(16) Lee, S. M.; Han, N.; Lee, R.; Choi, I. H.; Park, Y. B.; Shin, J. S.; Yoo, K. H. Real-Time Monitoring of 3D Cell Culture using a 3D Capacitance Biosensor. *Biosens. Bioelectron.* **2016**, *77*, 56−61.
(17) Simon, K. A.; Park, K. M.; Mosadegh, B.; Subramaniam, A. B.; Mazzeo, A. D.; Ngo, P. M.; Whitesides, G. M. Polymer-Based Mesh as Supports for Multi-Layered 3D Cell Culture and Assays. *Biomaterials* **2014**, *35*, 259−268.
(18) Derda, R.; Laromaine, A.; Mammoto, A.; Tang, S. K. Y.; Mammoto, T.; Ingber, D. E.; Whitesides, G. M. Paper-Supported 3D Cell Culture for Tissue-Based Bioassays. *Proc. Natl. Acad. Sci. U. S. A.* **2009**, *106*, 18457−18462.
(19) Lee, M. K.; Rich, M. H.; Baek, K.; Lee, J.; Kong, H. Bioinspired Tuning of Hydrogel Permeability-Rigidity Dependency for 3D Cell Culture. *Sci. Rep.* **2015**, *5*, 1−7.
(20) Lee, W.; Park, J. The Design of a Heterocellular 3D Architecture and its Application to Monitoring the Behavior of Cancer Cells in Response to the Spatial Distribution of Endothelial Cells. *Adv. Mater.* **2012**, *24*, 5339−5344.
(21) Chiew, G. G. Y.; Wei, N.; Sultania, S.; Lim, S.; Luo, K. Q. Bioengineered Three-Dimensional Co-Culture of Cancer Cells and Endothelial Cells: A Model System for Dual Analysis of Tumor Growth and Angiogenesis. *Biotechnol. Bioeng.* **2017**, *114*, 1865−1877.
(22) Swaminathan, S.; Ngo, O.; Basehore, S.; Clyne, A. M. Vascular Endothelial-Breast Epithelial Cell Coculture Model Created from 3D Cell Structures. *ACS Biomater. Sci. Eng.* **2017**, *3*, 2999−3006.
(23) Szot, C. S.; Buchanan, C. F.; Freeman, J. W.; Rylander, M. N. *In vitro* Angiogenesis Induced by Tumor-Endothelial Cell Co-Culture in Bilayered, Collagen I Hydrogel Bioengineered Tumors. *Tissue Eng., Part C* **2013**, *19*, 864−874.
(24) Patra, B.; Peng, Y. S.; Peng, C. C.; Liao, W. H.; Chen, Y. A.; Lin, K. H.; Tung, Y. C.; Lee, C. H. Migration and Vascular Lumen Formation of Endothelial Cells in Cancer Cell Spheroids of Various Sizes. *Biomicrofluidics* **2014**, *8*, 1−10.
(25) Pradhan, R.; Rajput, S.; Mandal, M.; Mitra, A.; Das, S. Electric Cell-Substrate Impedance Sensing Technique to Monitor Cellular Behaviours of Cancer Cells. *RSC Adv.* **2014**, *4*, 9432−9438.
(26) Hong, J.; Kandasamy, K.; Marimuthu, M.; Choi, C. S.; Kim, S. Electrical Cell-Substrate Impedance Sensing as a Noninvasive Tool for Cancer Cell Study. *Analyst* **2011**, *136*, 237−245.
(27) Szulcek, R.; Bogaard, H. J.; Amerongen, G. P. V. Electric Cell-Substrate Impedance Sensing for the Quantification of Endothelial Proliferation, Barrier Function, and Motility. *J. Visualized Exp* **2014**, *85*, 1−12.
(28) Kloss, D.; Kurz, R.; Jahnke, H. G.; Fischer, M.; Rothermel, A.; Anderegg, U.; Simon, J. C.; Robitzki, A. A. Microcavity Array (MCA)-Based Biosensor Chip for Functional Drug Screening of 3D Tissue Models. *Biosens. Bioelectron.* **2008**, *23*, 1473−1480.
(29) Eker, B.; Meissner, R.; Bertsch, A.; Mehta, K.; Renaud, P. Label-Free Recognition of Drug Resistance *via* Impedimetric Screening of Breast Cancer Cells. *PLoS One* **2013**, *8*, e57423.
(30) Wang, L.; Wu, Y. B.; Hu, T. L.; Guo, B. L.; Ma, P. X. Electrospun Conductive Nanofibrous Scaffolds for Engineering Cardiac Tissue and 3D Bioactuators. *Acta Biomater.* **2017**, *59*, 68−81.
(31) O'Brien, F. J. Biomaterials & Scaffolds for Tissue Engineering. *Mater. Today* **2011**, *14*, 88−95.
(32) Lo, C. M.; Lo, J. C.; Sato, P. Y.; Yeung, T. L.; Mok, S. C.; Yip, K. P. Monitoring of Ovarian Cancer Cell Invasion in Real Time with Frequency-Dependent Impedance Measurement. *Am. J. Physiol.* **2016**, *311*, 1040−1047.
(33) Zhu, P. F.; Ning, Y. X.; Yao, L. P.; Chen, M.; Xu, C. J. The Proliferation, Apoptosis, Invasion of Endothelial-Like Epithelial Ovarian Cancer Cells Induced by Hypoxia. *J. Exp. Clin. Canc. Res.* **2010**, *29*, 124.
(34) Walter-Yohrling, J.; Pratt, B. M.; Ledbetter, S.; Teicher, B. A. Myofibroblasts Enable Invasion of Endothelial Cells into Three-Dimensional Tumor Cell Clusters: a Novel *in vitro* Tumor Model. *Cancer Chemother. Pharmacol.* **2003**, *52*, 263−269.
(35) Hwang, S.; Tao, H.; Kim, D.; Cheng, H.; Song, J.; Rill, E.; Brenckle, M.; Panilaitis, B.; Won, S.; Kim, Y.; Song, Y.; Yu, K.; Ameen, A.; Li, R.; Su, Y.; Yang, M.; Kaplan, D.; Zakin, M.; Slepian, M.; Huang, Y.; Omenetto, F.; Rogers, J. A Physically Transient Form of Silicon Electronics. *Science* **2012**, *337*, 1640−1644.
(36) Hwang, S.; Lee, C.; Cheng, H.; Jeong, J.; Kang, S.; Kim, J.; Shin, J.; Yang, J.; Liu, Z.; Ameer, G.; Huang, Y.; Rogers, J. Biodegradable Elastomers and Silicon Nanomembranes/Nanoribbons for Stretchable, Transient Electronics, and Biosensors. *Nano Lett.* **2015**, *15*, 2801−2808.
(37) Hwang, S.; Kim, D.; Tao, H.; Kim, T.; Kim, S.; Yu, K.; Panilaitis, B.; Jeong, J.; Song, J.; Omenetto, F.; Rogers, J. Materials and Fabrication Processes for Transient and Bioresorbable High-Performance Electronics. *Adv. Funct. Mater.* **2013**, *23*, 4087−4093.
(38) Kang, S. K.; Murphy, R. K. J.; Hwang, S. W.; Lee, S. M.; Harburg, D. V.; Krueger, N. A.; Shin, J. H.; Gamble, P.; Cheng, H. Y.; Yu, S.; Liu, Z. J.; McCall, J. G.; Stephen, M.; Ying, H. Z.; Kim, J.; Park, G.; Webb, R. C.; Lee, C. H.; Chung, S. J.; Wie, D. S.; Gujar, A. D.; Vemulapalli, B.; Kim, A. H.; Lee, K. M.; Cheng, J. J.; Huang, Y. G.; Lee, S. H.; Braun, P. V.; Ray, W. Z.; Rogers, J. A. Bioresorbable Silicon Electronic Sensors for the Brain. *Nature* **2016**, *530*, 71−75.
(39) Xu, L. Z.; Gutbrod, S. R.; Ma, Y. J.; Petrossians, A.; Liu, Y. H.; Webb, R. C.; Fan, J. A.; Yang, Z. J.; Xu, R. X.; Whalen, J. J.; Weiland, J. D.; Huang, Y. G.; Efimov, I. R.; Rogers, J. A. Materials and Fractal Designs for 3D Multifunctional Integumentary Membranes with Capabilities in Cardiac Electrotherapy. *Adv. Mater.* **2015**, *27*, 1731−1735.
(40) Kim, D. H.; Rogers, J. A. Stretchable Electronics: Materials Strategies and Devices. *Adv. Mater.* **2008**, *20*, 4887−4892.
(41) Yang, Y.; Gao, W. Wearable and Flexible Electronics for Continuous Molecular Monitoring. *Chem. Soc. Rev.* **2019**, *48*, 1465−1491.

DOI: 10.1021/acsnano.9b02291
ACS Nano XXXX, XXX, XXX−XXX